A new model for the absorption coefficient of narrow-gap (Hg,Cd)Te that simultaneously considers band tails and band filling

K. H. Herrmann, M. Happ, H. Kissel, K.-P. Möllmann, and J. W. Tomm
Fachbereich Physik der Humboldt-Universität zu Berlin, Institut für Festkörperphysik, Invalidenstrasse 110, O-1140 Berlin, Germany

C. R. Becker, M. M. Kraus, S. Yuan,[a] and G. Landwehr
Physikalisches Institut der Universität Würzburg, MBE-Labor, Am Hubland, W-8700 Würzburg, Germany

(Received 13 August 1992; accepted for publication 14 December 1992)

A semiempirical model is presented that correlates the broadening of the absorption edge with both transitions below the energy gap and with transitions by the Kane band model. This model correctly fits both the absorption and luminescence spectra of narrow-gap (Hg,Cd)Te samples that have been grown by the traveling heater method as well as by molecular-beam epitaxy. The accuracy of the band-gap determination is enhanced by this model.

I. INTRODUCTION

Narrow-gap (Hg,Cd)Te is an important material used in infrared detectors that has a number of physical properties of considerable interest: The small effective mass of the electrons [m_n, $m_{lh} \cong 0.008 m_0 \ll 0.44 m_0 \cong m_{hh}$ for $x=0.2$ at $T=77$ K (Ref. 1) results in rather large quantum-size effects in structures with reduced dimensionality and with pronounced Landau quantization in a magnetic field. Furthermore, the mixed crystal system is seen as a model substance for studying alloy disorder effects as a function of the energy gap.

The absorption coefficient of (Hg,Cd)Te can be empirically described by different relationships for different spectral regions. Above the energy gap E_g where the Kane band structure is valid, the absorption coefficient follows a modified square-root law,[2] and at energies near E_g it exhibits an exponential Urbach tail. Both regions have been investigated in numerous experimental studies, and a large amount of empirical data already exists (see, e.g., Ref. 3).

The energy dependence of the absorption coefficient of the Urbach tail may be described by

$$\alpha(\hbar\omega) = \alpha(\hbar\omega_0) \exp[(\hbar\omega - \hbar\omega_0)/W_0]. \quad (1)$$

Here W_0 is a parameter that is an indication of the width of the tail and $\hbar\omega_0$ a parameter that defines the transition from the modified square-root law to an exponential dependence. Both W_0 and $\hbar\omega_0$ are experimental parameters that can be determined from absorption measurements either directly from transmission spectra or indirectly from photoconductivity or the spectral response of a photodiode; see, e.g., Ref. 4.

The mechanisms that contribute to broadening have been analyzed in Refs. 4 and 5. An analysis of the temperature dependence of W_0 resulted in the following relationship:

$$W_0(T) = E_p + \sigma k_B T. \quad (2)$$

E_p, which will be referred to as "permanent broadening" remaining at zero temperature, is independent of temperature. Since the same broadening parameter W_0 is obtained in experiments with bipolar photogeneration, we proposed earlier the hypothesis[6] that the exponential tail is caused by states that have been shifted from the valence and conduction bands to energies within the gap. The composition dependence of the broadening $W_0(x)$ of high-quality crystals grown by the traveling heater method (THM) near thermodynamic equilibrium correlates well with the disorder function $W_0 \sim x(1-x)$.[7] This leads us to the hypothesis that E_p is due to alloy disorder. In contrast to Fuchs and Koidl,[8] charge-carrier localization due to fluctuating band edges will not be considered here.

The temperature-dependent contribution to W_0 is probably due to more than one mechanism, judging by the individual sample results. For example, experimental evidence has been given by Herrmann and co-workers[7] that acceptor levels contribute to the temperature dependence of W_0. In this article a quantitative model for optical transitions in narrow-gap (Hg,Cd)Te is presented, which describes in a uniform manner normal optical absorption as well as nonequilibrium phenomena such as luminescence and pumped absorption. This required a description of band filling in the spectral region where the Urbach tail is present. In addition, this model accurately describes the corresponding spectra of samples with different disorder structure or other parameters as judged by their exponential Urbach tail. Thus, an investigation of the physical nature of the energy states which cause the Urbach tail is possible.

II. EMPIRICAL DATA AND SEMIEMPIRICAL MODEL

In the following analysis, optical absorption near the interband edge is attributed to band-to-band transitions that conserve $\mathbf{k}$.[2] Excitonic contributions can be completely neglected according to arguments concerning magnetophotoluminescence[9] and temperature-dependent broadening.[7]

[a]On leave from Shanghai Institute of Technical Physics, Academia Sinica, 420 Zhong Shan Bei Yi Road, Shanghai, People's Republic of China.

 0021-8979/93/073486-07$06.00

Up to now the separation of the exponential Urbach component, Eq. (1), from the square-root dependence, has been carried out by requiring that the absorption coefficient is continuous at the transition but without considering band filling.[8] This is reflected in the value of the absorption coefficient at the transition between exponential and square-root dependence[10] compared to the value usually assumed: $\alpha = 1000\ \mathrm{cm}^{-1}$. This implies, apart from corrections for k-dependent matrix elements, that the tail can be described as due to a modified density of states at $E < E_g$ in the disordered crystal.

However, in order to establish a model of the spectral region below E_g for doped samples or for a nonequilibrium situation we have to consider how band filling will influence interband transitions that involve states in the tail. If we assume that these tail states originated in one of the bands, then we should use a continuous extrapolation of the real absorption coefficient [absorption coefficient multiplied by a band-filling factor (BFF)] for all kinds of transitions. Because this band-filling factor depends on the energy at the k value where these transitions take place, a suitable average over light and heavy holes must be used. As a first approximation the band-filling factor for heavy-hole to conduction-band transitions will be used:

$$\mathrm{BFF} = f(\mathrm{BFF}_{\mathrm{lh}}, \mathrm{BFF}_{\mathrm{hh}}) \approx \mathrm{BFF}_{\mathrm{hh}} . \qquad (3)$$

Equation (3) implies that the tail states above the valence-band edge are mainly due to the heavy hole. This is in accordance with the large ratio of the density-of-state masses and with the observation that for HgTe/CdTe heterostructures the valence-band offset is only about 20% of the gap difference.

The assumption that the Urbach region can be described by Eq. (1) multiplied by the band-filling factor given by Eq. (3) is confirmed by pumped absorption experiments when the excitation is resonant with the tail states, as described in Sec. IV C.

The spectral dependence of the absorption coefficient well above E_g is described by the Kane band structure as outlined by Anderson.[2,11] We applied his formula to the nonequilibrium case (existence of quasi-Fermi levels), i.e., to luminescence and pumped absorption experiments, in a previous publication.[7] Here we shall use similar notation as in Refs. 7 and 11.

The main assumption of these considerations is that permanent broadening is caused by real-space fluctuations of the band edges due to alloy disorder. The resulting potential valleys are considered to be macroscopic crystalline regions when compared to the spatial expansion of the trapped carrier wave functions. The combined density of states of an inhomogeneous crystalline region, as defined above, should be constant for various degrees of alloy disorder resulting from different growth methods of the samples.

The procedure used to fit the optical spectra is very simple. The following input parameters are used: the energy gap E_g, effective charge-carrier temperature T_e, tail parameter W_0, and minority- and majority-carrier concentrations which define the positions of the quasi-Fermi levels. Both $\hbar\omega_0$ (the transition point between the exponential and square-root regions) and $\alpha(\hbar\omega_0)$ were determined by fulfilling the demand for a continuous transition between the exponential and square-root regions when in equilibrium or, in other words, without exitation.

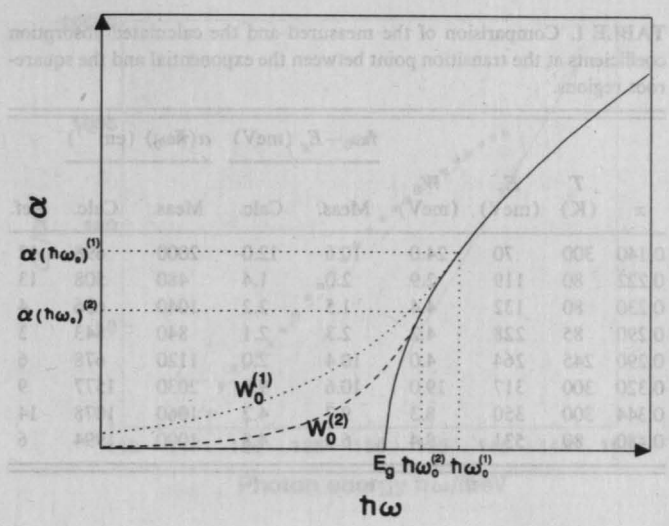

FIG. 1. Schematic drawing of the absorption coefficient vs photon energy $\hbar\omega$. $W_0 = 0$ (absorption edge without broadening) (solid line); $W_0^{(1)}$ ($W_0^{(1)} > W_0^{(2)} > 0$) (dotted line); $W_0^{(2)}$ (dashed line).

Employing this model, one finds that larger tail energies W_0 are accompanied by larger spectral distances between E_g and $\hbar\omega_0$ and higher values of $\alpha(\hbar\omega_0)$, as is already empirically known (see Fig. 1). Figure 2 displays a calculation applying our model with relevant sample parameters. Experimental data including W_0 and $\alpha(\hbar\omega_0)$ for a large variety of samples published by several authors are

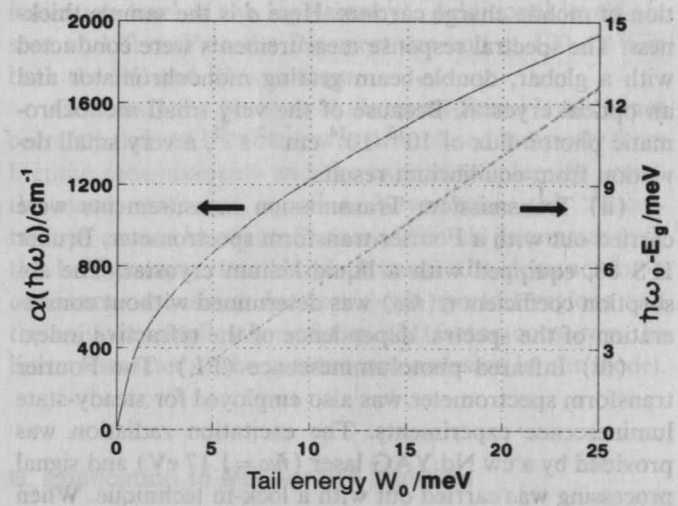

FIG. 2. Value of the absorption coefficient at the energy $\hbar\omega_0$ where the Urbach tail meets the modified square-root law according to our fit procedure (left-hand-side scale) vs tailing energy W_0 according to Eq. (1). The right-hand-side axis indicates the difference between $\hbar\omega_0$ and the energy gap E_g. The values of the parameters used are: $x = 0.27$, $T = 20$ K, $E_g = 181.35$ meV, $Q_p = 20$ meV, $Q_n = -(E_G + Q_p)$ (notations according to Refs. 7 and 11).

TABLE I. Comparision of the measured and the calculated absorption coefficients at the transition point between the exponential and the square-root regions.

				$\hbar\omega_0 - E_g$ (meV)		$\alpha(\hbar\omega_0)$ (cm^{-1})		
x	T (K)	E_g (meV)	W_0 (meV)	Meas.	Calc.	Meas.	Calc.	Ref.
0.140	300	70	24.0	10.6	12.0	2000	698	12
0.222	80	119	2.9	2.0	1.4	480	508	13
0.230	80	132	4.4	1.5	2.2	1040	656	4
0.290	85	228	4.2	2.3	2.1	840	843	3
0.290	245	264	4.0	10.4	2.0	1120	678	6
0.320	300	317	19.0	10.6	9.8	2030	1577	9
0.344	300	350	8.3	9.7	4.2	1060	1078	14
0.480	80	531	9.4	6.0	4.8	1000	1994	6

compared with values calculated from our model in Table I. Note the good agreement between the two sets of data.

III. EXPERIMENT

The samples investigated were grown by the traveling heater method (THM) and molecular-beam epitaxy (MBE), as described in Refs. 15 and 16. Both kinds of samples were characterized by a number of standard methods which include transport measurements, photoconductive decay, and chemical analysis. These experiments provide the data necessary to determine the input parameters such as the Fermi level and quasi-Fermi levels in the absence of excitation (absorption and photoconductivity) as well as with excitation (luminescence). The main techniques employed in this study are as follows.

(i) Steady-state photoconductivity (PC): The form or structure of the absorption edge when $\alpha d < 1$ can be obtained from the spectral response of the interband generation of mobile charge carriers. Here d is the sample thickness. The spectral response measurements were conducted with a globar, double-beam grating monochromator and an optical cryostat. Because of the very small monochromatic photon flux of 10^{13}–10^{14} $cm^{-2}\,s^{-1}$, a very small deviation from equilibrium results.

(ii) Transmission: Transmission measurements were carried out with a Fourier transform spectrometer, Bruker IFS 88, equipped with a liquid-helium cryostat. The absorption coefficient $\alpha(\hbar\omega)$ was determined without consideration of the spectral dependence of the refractive index.

(iii) Infrared photoluminescence (PL): The Fourier transform spectrometer was also employed for steady-state luminescence experiments. The excitation radiation was provided by a cw Nd:YAG laser ($\hbar\omega = 1.17$ eV) and signal processing was carried out with a lock-in technique. When high excitation levels were required, a Q-switched Nd:YAG laser ($\tau_{FWHM} = 80$ ns, where FWHM denotes the full width at half-maximum) was employed as an excitation source, spectral discrimination and detection were accomplished with a conventional double monochromator and a fast (Hg,Cd)Te photodiode; for details, see Ref. 17.

(iv) Pumped absorption (PA): PA measurements were done with a pump and probe method. A Q-switched CO_2 laser ($\tau_{FWHM} = 220$ ns) was employed both as an excitation source as well as a source for the transmission measurement. The 116.9 meV emission line was selected by means of a grating and the intensity of this laser line was attenuated with a set of filters, whose transmittances are independent of wavelength in the CO_2-laser frequency range. The samples were cooled in an optical cryostat, and a (Hg,Cd)Te photodiode was used as a detector.

IV. RESULTS AND DISCUSSION

A. Application to THM-grown samples

A PC spectrum of a THM-grown sample is displayed in Fig. 3(a) and a PL spectrum as well as a transmission spectrum near the energy gap of the same sample at $T = 4.2$ K are shown in Fig. 3(b).

Two values for W_0 are given in Fig. 3(a). The value of 3.8 meV (dashed line) fits the PC spectrum for the entire region from 130 to 150 meV whereas the lower value of 2.1 meV (solid line) gives a better fit but only for the region between 145 and 150 meV. Using both of these values along with the corresponding values of $\hbar\omega_0$ and $\alpha(\hbar\omega_0)$, which are given in the figure caption, the spectral dependence of the absorption coefficient was calculated as described in Sec. II.

This absorption coefficient was used to fit the luminescence spectrum obtained at higher excitation levels which is shown on the right-hand side in Fig. 3(b). The dashed line corresponds to the larger value of W_0 and the solid line to the smaller value. Note the very good agreement between the measured curve and calculated curves for the spectral regions mentioned above, i.e., the dashed line fits better overall and especially the low-energy region whereas the solid line fits better at higher energies. The effective carrier temperature T_e used in the fit of the high-energy tail of the PL spectrum was determined from a semilogarithmic plot of the luminescence. Obviously the cw-luminescence spectrum with a weaker excitation [dotted line in Fig. 3(b)] is due to transitions involving levels in the energy gap and does not include interband contributions.

Figure 3(c) shows the absorption coefficient as determined from a transmission spectrum (squares). The dashed line that falls near the experimental absorption coefficient is the result of Eq. (1) with $\hbar\omega_0$ and $\alpha(\hbar\omega_0)$ as determined from the luminescence line shape fit using a value for the tail parameter W_0 of 3.8 meV. The solid line results from Eq. (1) when $W_0 = 2.1$ meV, which fits the luminescence line shape at higher energies. We cannot compare the transmission data with this line at higher energies because its thickness ($d = 500$ μm) does not permit an accurate determination of larger values of the absorption coefficient. Both lines represent the absorption coefficient without a dynamic BM shift. This is correct for transmission measurements because of the low excitation level compared to levels used in luminescence experiments.

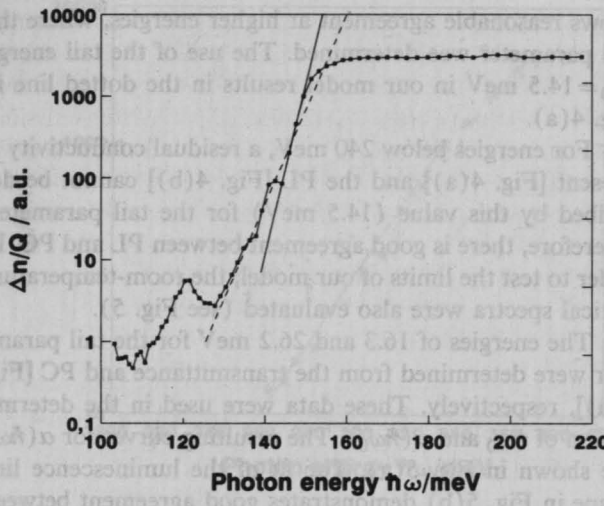

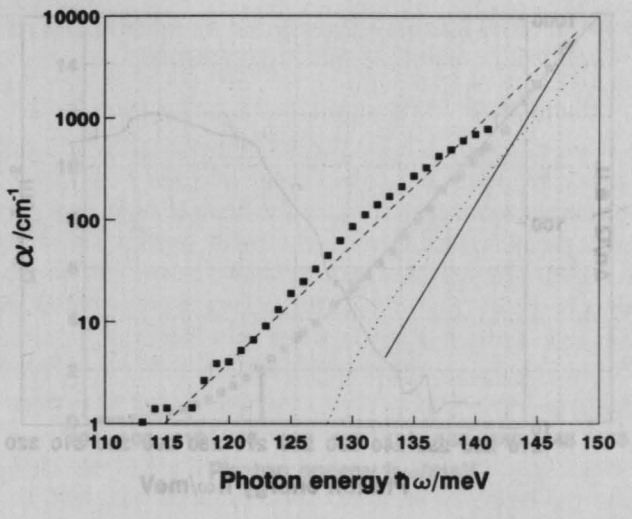

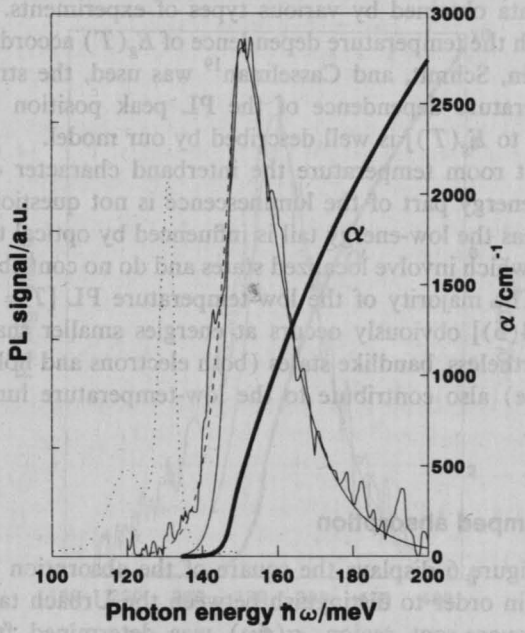

FIG. 3. Optical spectra and empirical results using the fitting procedure for a THM-grown sample at $T=4.2$ K with $x=0.2515$ and $E_g=146.5$ meV. (a) PC spectrum: $W_0=2.1$ meV (solid line); $W_0=3.8$ meV (dashed line). (b) PL spectra (PL signal in arbitrary units) at low (several W cm^{-2}) and high (50 kW cm^{-2}) excitation densities are shown as a dotted line on the left-hand side and a solid line on the right-hand side, respectively. The solid line represents a line-shape fit using $W_0=2.1$ meV [see Fig. 2(a)] and the dashed line a fit for $W_0=3.8$ meV. Using these two values in Eq. (1) results in $\hbar\omega_0=147.5$ and 148.3 meV as well as in $\alpha(\hbar\omega_0)=503.1$ and 649.2 cm^{-1}, respectively. An effective carrier temperature of $T_e=130$ K was determined from the high-excitation density spectrum on the right-hand side. A diffusion length of 10 μm (from transport and lifetime measurement) was used in calculation of the reabsorption. The position of the quasi-Fermi levels, Q_n and Q_p, was -10 meV. The absorption coefficient behavior includes the dynamic BM shift. The photon energy is shown on the right-hand side. (c) Absorption coefficients vs photon energy. Squares denote data calculated from the transmission measurement. Both straight lines represent $\alpha(\hbar\omega)$ according to Eq. (1) for both values of the parameters without dynamic BM shift. Solid line: $W_0=2.1$ meV, $\alpha(\hbar\omega_0)=511$ cm^{-1}, $\hbar\omega_0=147.6$ meV; dashed line: $W_0=3.8$ meV, $\alpha(\hbar\omega_0)=680$ cm^{-1}, $\hbar\omega_0=148.4$ meV. The dotted line is a modification of the dashed line when one takes into account the dynamic BM shift as is usually done for PL measurements.

If one takes into account a realistic excitation level for luminescence, but no degeneracy, then a dynamic Burstein–Moss (BM) shift must be taken into consideration which shifts the dashed line ($W_0=3.8$ meV) to the dotted one. This spectral dependence of the absorption coefficient including a dynamic BM shift describes the absorption of the excited material and is also plotted in Fig. 3(b) as a solid line.

In order to further test the consistency of our model the PC spectrum was simulated. Assuming a diffusion length of 10 μm in order to describe the recombination, the absorption coefficient has a value of 1000 cm^{-1} at e^{-1} times the plateau value which occurs at about 150 meV. An extrapolation of the lines in Fig. 3(c) also reaches 1000 cm^{-1} at about this energy.

Therefore, our model consistently describes all three sets of experimental data (PL, transmittance, and PC). The smaller value of the broadening parameter describes the band tails due to alloy disorder, whereas the larger one describes an envelope which contains two acceptor levels in the PC spectrum at 136 meV (probably a hydrogenlike acceptor) and at 143 meV (probably caused by the first ionization level of the Hg vacancy). Additional levels are seen at 130 meV in the PL spectrum and at 120 meV in both the PC and PL spectrum.

Obviously the position of the quasi-Fermi levels is not correctly defined because it was determined indirectly from lifetime measurements and the excitation intensity versus the steady-state rate equation. Nevertheless this "uncertainity" cannot be misused as an additional parameter to fit the luminescence line shape, because the demand for a continuous transition between both spectral regions and the uniform application of the BM factor conserves the linear character of the spontaneous emission in our model.

B. Application to MBE-grown samples

The procedure as described above was also applied to the optical spectra obtained from MBE-grown samples. The PL intensities of these samples are comparable to those for THM-grown samples with the exception that the full width at half-maximum (FWHM) is significantly larger. In addition the application of pulsed, high-intensity

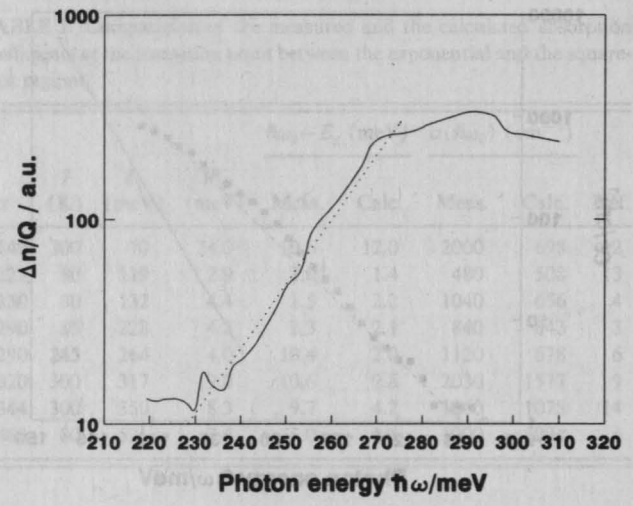

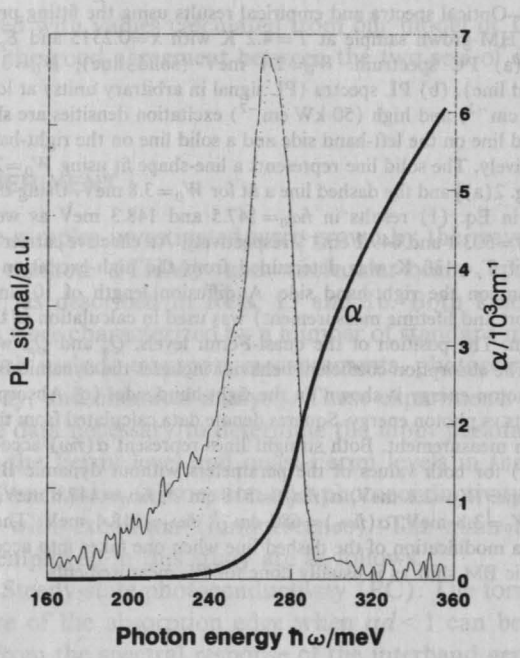

FIG. 4. Optical spectra and empirical results using the fitting procedure for a MBE-grown sample at $T=18$ K with $x=0.328$ and $E_g=276.6$ meV. (a) PC spectrum: The dotted line indicates the tail energy $W_0=14.5$ meV. (b) PL spectrum with an excitation density of several W cm^{-2}. The line-shape fit takes into account the tail energy as determined in (a). This results in $\hbar\omega_0=283.8$ meV and $\alpha(\hbar\omega_0)=1814$ cm^{-1}. The solid line indicates values for $\alpha(\hbar\omega)$ which include the dynamic BM shift. The effective carrier temperature is 48 K and a diffusion length of 3.0 μm describes the reabsorption in the comparable thin ($d=9.2$ μm) sample. For the quasi-Fermi levels we used $Q_n=0$ meV and $Q_p=-7$ meV.

excitation does not shift the broadened luminescence as expected from charge-carrier heating. These are the main differences to the behavior of the THM samples described above. Nevertheless, we note that THM samples often exhibit interband luminescence for both low- and high-excitation levels[17,18] and, therefore, do not normally exhibit a shift as large as shown in Fig. 3(b).

Figure 4(a) displays the PC spectrum of an MBE sample that exhibits a tail parameter of 14.5 meV at $T=18$ K. The PL line-shape fit using our model [see Fig. 4(b)] shows reasonable agreement at higher energies, where the tail parameter was determined. The use of the tail energy $W_0=14.5$ meV in our model results in the dotted line in Fig. 4(a).

For energies below 240 meV, a residual conductivity is present [Fig. 4(a)] and the PL [Fig. 4(b)] cannot be described by this value (14.5 meV) for the tail parameter. Therefore, there is good agreement between PL and PC. In order to test the limits of our model, the room-temperature optical spectra were also evaluated (see Fig. 5).

The energies of 16.3 and 26.2 meV for the tail parameter were determined from the transmittance and PC [Fig. 5(a)], respectively. These data were used in the determination of $\hbar\omega_0$ and $\alpha(\hbar\omega_0)$. The resulting curves for $\alpha(\hbar\omega)$ are shown in Fig. 5(a). The fit of the luminescence line shape in Fig. 5(b) demonstrates good agreement between the data obtained by various types of experiments. Even though the temperature dependence of $E_g(T)$ according to Hansen, Schmit, and Casselman[19] was used, the stronger temperature dependence of the PL peak position [compared to $E_g(T)$] is well described by our model.

At room temperature the interband character of the high-energy part of the luminescence is not questionable, whereas the low-energy tail is influenced by optical transitions which involve localized states and do no contribute to PC. The majority of the low-temperature PL [$T=18$ K, Fig. 4(b)] obviously occurs at energies smaller than E_g. Nevertheless, bandlike states (both electrons and holes are mobile) also contribute to the low-temperature luminescence.

C. Pumped absorption

Figure 6 displays the square of the absorption coefficient in order to distinguish between the Urbach tail and the square-root region. $\alpha(\hbar\omega)$ was determined from a transmission measurement using an IFS 88 Fourier transform spectrometer. We chose the relevant parameters for the sample ($x=0.212$, $T=77$ K, $d=24$ μm) in such a way that the absorption coefficient at the CO_2-laser photon energy ($\hbar\omega=116.9$ meV, indicated by an arrow) falls in the low-energy tail of the absorption edge.

Figure 7 displays the dependence of the absorption coefficient on quantum flux density for excitation resonant with the tail using a Q-switched CO_2 laser for the same sample parameters. The rectangles are the measured values. For quantum flux densities Q above 2×10^{21} cm^{-2} s^{-1} we obtained a decrease in the absorption coefficient, whereas it remained constant ($\alpha\approx1700$ cm^{-1}) for $Q<2\times10^{21}$ cm^{-2} s^{-1}. The curve in Fig. 7 is a fit with the following assumptions.

(a) Spatial distribution of excitation: The sample under consideration has an acceptor concentration of 9.1×10^{15} cm^{-3}. Thus, it follows that the minority-carrier diffusion length is about $L_n=25$ μm. Because the sample thickness is $d=24$ μm we can assume bulk excitation.

(b) Steady-state nonequilibrium carrier concentration: The excitation was provided by a Q-switched CO_2 laser with a relatively large τ_{FWHM} of 220 ns compared with the

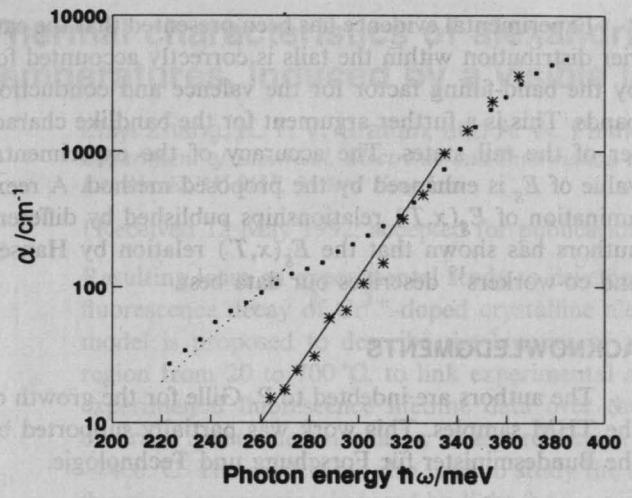

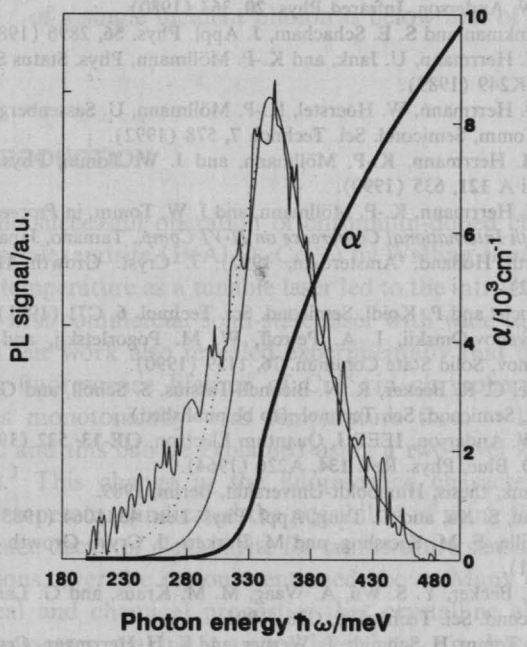

FIG. 5. Optical spectra and empirical results using the fitting procedure for the MBE-grown sample discussed in Fig. 4 at room temperature with $x=0.328$ and $E_g=328.5$ meV. (a) $\alpha(\hbar\omega)$ determined from transmittance (points) and from PC spectrum (stars). The slopes are 16.3 meV (solid line) and 26.2 meV (dotted line) for the transmission and PC spectra, respectively. The corresponding $\hbar\omega_0$ and $\alpha(\hbar\omega_0)$ values are 336.9 and 341.6 meV as well as 1480 and 1862 cm^{-1}, respectively. (b) Two fits of the PL line shape using the tail energies mentioned above. The values of the resulting parameters are given above in (a). A diffusion length of 1 μm defines the reabsorption and the carrier temperature was determined to be $T_e=320$ K. For the quasi-Fermi level positions we used $Q_n=-5$ meV and $Q_p=-230$ meV. The solid line indicates values for $\alpha(\hbar\omega)$ which include the dynamic BM shift.

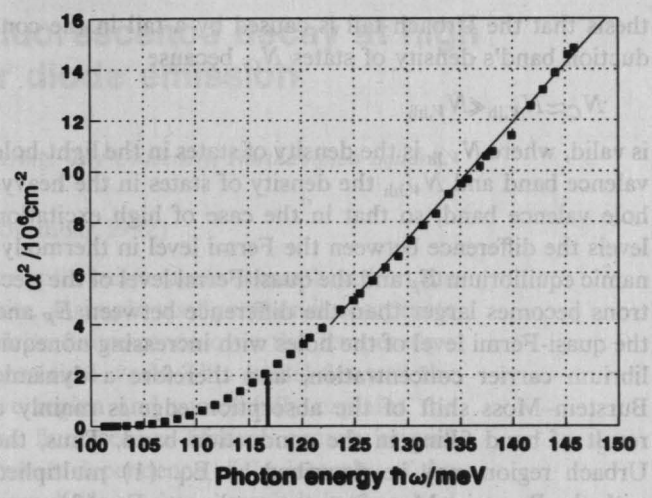

FIG. 6. The square of the absorption coefficient vs photon energy. The arrow indicates a CO_2-laser photon energy of about 117 meV. Relevant parameters of the sample are: $x=0.212$, $d=24$ μm, and $T=77$ K.

lifetime of the generated nonequilibrium carriers. Therefore, it is justifiable to assume a quasistationary nonequilibrium carrier concentration at the time of the measurement.

(c) Dynamic Burstein–Moss shift: The resulting decrease in absorption coefficient for increasing quantum flux densities above 2×10^{21} $cm^{-2}\,s^{-1}$ (due to band filling in the Urbach region) led us to the hypothesis that the observed optical transitions are k-conserving interband transitions between states of the valence bands and the conduction band; i.e., in order to describe the displacement of the absorption edge to higher photon energies we must multiply Eq. (1) with a Burstein–Moss factor as given in Eq. (3).

Note the very good agreement between the measured values and the calculated curve in Fig. 7 which is a verification in particular of assumption (c). This agreement was attainable only with this assumption. This means that the states responsible for the Urbach tail are bandlike states and that the Urbach region may be described by Eq. (1) multiplied with the Burstein–Moss factor according to Eq. (3). This result of our investigation led us to the hypo-

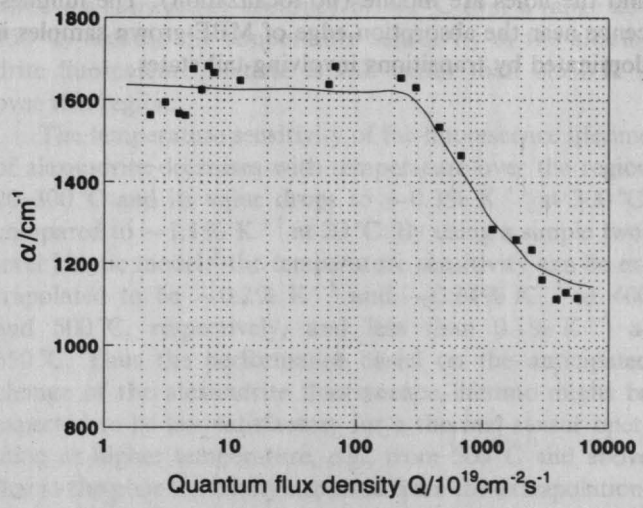

FIG. 7. The absorption coefficient of the same sample as in Fig. 6 vs quantum flux density for excitation resonant with the tail using a CO_2 laser. The rectangles are measured values whereas the curve is a fit in which Eq. (3) is used to describe the dynamic BM shift for tail states ($x=0.212$, $d=24$ μm, and $T=77$ K).

thesis that the Urbach tail is caused by a tail in the conduction band's density of states N_C, because

$$N_C \approx N_{V,\mathrm{lh}} \ll N_{V,\mathrm{hh}}$$

is valid, where $N_{V,\mathrm{lh}}$ is the density of states in the light-hole valence band and $N_{V,\mathrm{hh}}$ the density of states in the heavy-hole valence band, so that in the case of high excitation levels the difference between the Fermi level in thermodynamic equilibrium E_F and the quasi-Fermi level of the electrons becomes larger than the difference between E_F and the quasi-Fermi level of the holes with increasing nonequilibrium carrier concentration, and therefore a dynamic Burstein–Moss shift of the absorption edge is mainly a result of band filling in the conduction band. Thus, the Urbach region may be described by Eq. (1) multiplied with the Burstein–Moss factor according to Eq. (3).

V. CONCLUSIONS

A well-defined empirical model was presented that describes the spectral dependence of the absorption coefficient in narrow-gap (Hg,Cd)Te with a CdTe mole fraction between 0.2 and 0.3. This model quantitatively fits the spectra in the region near the absorption edge from photoluminescence, photoconductivity, as well as transmission experiments. This is true for samples exhibiting both p and n conductivity, and with different values for the tail parameters. In addition, the temperature dependence of the spectra is correctly described.

THM samples grown near thermodynamic equilibrium have a small permanent tail energy (about 2 meV) whereas MBE-grown samples exhibit values of about 14 meV. Nevertheless, the luminescence intensities do not differ appreciably. This indicates that the tail states (bandlike as well as localized) do not contribute significantly to nonradiative recombination processes. Tail states which have a bandlike character contribute to the spectra of all of the experiments conducted at all temperatures, because both the electrons and the holes are mobile (no localization). The luminescence near the absorption edge of MBE-grown samples is dominated by transitions involving tail states.

Experimental evidence has been presented that the carrier distribution within the tails is correctly accounted for by the band-filling factor for the valence and conduction bands. This is a further argument for the bandlike character of the tail states. The accuracy of the experimental value of E_g is enhanced by the proposed method. A reexamination of $E_g(x,T)$ relationships published by different authors has shown that the $E_g(x,T)$ relation by Hansen and co-workers[19] describes our data best.

ACKNOWLEDGMENTS

The authors are indebted to P. Gille for the growth of the THM samples. This work was partially supported by the Bundesminister für Forschung und Technologie.

[1] M. C. Gold and D. A. Nelson, J. Vac. Sci. Technol. A **4**, 2040 (1986).
[2] W. W. Anderson, Infrared Phys. **20**, 363 (1980).
[3] E. Finkman and S. E. Schacham, J. Appl. Phys. **56**, 2896 (1984).
[4] K. H. Herrmann, U. Jank, and K.-P. Möllmann, Phys. Status Solidi A **114**, K249 (1989).
[5] K. H. Herrmann, W. Hoerstel, K.-P. Möllmann, U. Sassenberg, and J. W. Tomm, Semicond. Sci. Technol. **7**, 578 (1992).
[6] K. H. Herrmann, K.-P. Möllmann, and J. W. Tomm, Phys. Status Solidi A **121**, 635 (1990).
[7] K. H. Herrmann, K.-P. Möllmann, and J. W. Tomm, in *Proceedings of the 5th International Conference on II-VI Comp.*, Tamano, Japan, 1991 (North Holland, Amsterdam, 1992); J. Cryst. Growth **117**, 758 (1992).
[8] F. Fuchs and P. Koidl, Semicond. Sci. Technol. **6**, C71 (1991).
[9] A. Ivanov-Omskii, I. A. Petroff, W. M. Pogorletskij, and V. A. Smirnov, Solid State Commun. **76**, 1159 (1990).
[10] L. He, C. R. Becker, R. N. Bicknell-Tassius, S. Scholl, and G. Landwehr, Semicond. Sci. Technol. (to be published).
[11] W. W. Anderson, IEEE J. Quantum Electron. **QE-13**, 532 (1977).
[12] M. D. Blue, Phys. Rev. **134**, A226 (1964).
[13] U. Jank, thesis, Humboldt-Universität, Berlin, 1989.
[14] J. Chu, S. Xu, and D. Tang, Appl. Phys. Lett. **43**, 1064 (1983).
[15] P. Gille, F. M. Kiessling, and M. Burkert, J. Cryst. Growth **114**, 77 (1991).
[16] C. R. Becker, Y. S. Wu, A. Waag, M. M. Kraus, and G. Landwehr, Semicond. Sci. Technol. **6**, C76 (1991).
[17] J. W. Tomm, H. Schmidt, L. Werner, and K. H. Herrmann, Cryst. Res. Technol. **25**, 1069 (1990).
[18] L. Werner, J. W. Tomm, J. Tilgner, and K. H. Herrmann, J. Cryst. Growth **101**, 787 (1990).
[19] G. L. Hansen, J. L. Schmit, and T. N. Casselman, J. Appl. Phys. **53**, 7099 (1982).

Thermal characteristics of alexandrite fluorescence decay at high temperatures, induced by a visible laser diode emission

Zhiyi Zhang, K. T. V. Grattan, and A. W. Palmer
Department of Electrical, Electronic and Information Engineering, City University, Northampton Square, London EC1V 0HB, United Kingdom

(Received 12 May 1992; accepted for publication 4 November 1992)

Resulting from an experimental study to develop a fiber-optic temperature sensor based on the fluorescence decay of Cr^{3+}-doped crystalline alexandrite, a simple configurational coordinate model is proposed to describe the kinetics of alexandrite fluorescence over the temperature region from 20 to 700 °C, to link experimental and theoretical work. This model fits well the experimental fluorescence lifetime data over the above region and successfully explains the observed phenomenon that a sharp reduction in the fluorescence lifetime occurs beyond ~400 °C. The model was also used to study the temperature dependence of the intensity of the fluorescence emission induced by light from a visible laser diode, and as a result it is suggested that a phonon-assisted absorption is involved in a specific absorption process, where the energy of a single incident photon is below that of the primary absorption band $^4T_2$.

I. INTRODUCTION

The successful operation of chromium-doped chrysoberyl or alexandrite ($BeAl_2O_4$:Cr^{3+}) by Walling *et al.*[1-3] at room temperature as a tunable laser led to the introduction of the first commercial solid-state laser with wide tunability.[4] Their work also revealed experimentally that the intrinsic fluorescence lifetime of Cr^{3+} in chrysoberyl decreases monotonically with temperature from −120 to 220 °C and this can be explained using a two-level kinetic model.[3] This change in the fluorescence characteristics with temperature indicated the possibility of using the fluorescence decay of alexandrite for temperature sensing applications, over the region mentioned above. Many of the physical and chemical properties that crystalline alexandrite possesses, making it a good laser host, e.g., hardness, strength, chemical stability, and high thermal conductivity (two-thirds of that of ruby and twice that of YAG), also make it favorable as a temperature transducer material. In addition, the broad absorption spectrum of alexandrite, which ranges from 380 to 680 nm, allows a low-cost, compact light source, such as a visible light-emitting diode (LED) or diode laser to be used to induce the fluorescence and the use of such a pumping source, makes the system highly acceptable for applications outside the laboratory environment where the device can be powered by batteries.

The fluorescence spectrum of alexandrite is comprised of a sharp *R*-line emission superimposed on a broad vibronic emission background, as shown in Fig. 1. In this material, the energy difference between the lowest members of $^4T_2$ (responsible for broadband emission) and ^2E (*R*-line radiation) is about 754 cm^{-1} (Ref. 3) or 0.0935 eV at room temperature [in contrast to 2300 cm^{-1}, the energy difference ($^4T_2$−^2E) for ruby[5]]. This energy difference allows the higher degree of repopulation of the $^4T_2$ level due to the thermal elevation of the excited Cr^{3+} ions from the metastable ^2E level, compared to that in the case of ruby, and consequently enables potentially a higher degree of broadband emission. The lifetime of the $^4T_2$ level, approximately 10 μs, is much shorter than that of the long-lived ^2E level, so that thermally activated repopulation between the $^4T_2$ and ^2E levels results in a highly sensitive change of alexandrite fluorescence lifetime with temperature from −100 °C to room temperature, and the rate of decrease of the fluorescence lifetime can be greater than 1% K^{-1} over the above temperature region.

The use of the fluorescence from alexandrite for temperature sensing was first reported by some of the authors.[6,7] It had been the subject of a limited temperature study, using a low-power LED or a modulated He-Ne laser excitation source. Though the poor signal-to-noise ratio obtained with the use of a LED light source[7] or the bulky optical modulation device which was part of the system using a He-Ne laser[6] limited the practical utility of the previous scheme, under laboratory conditions it did achieve a satisfactory accuracy of ±1 °C over a range 20–150 °C, because the temperature sensitivity of the alexandrite fluorescence lifetime is still better than 0.5% K^{-1} over this region.

The temperature sensitivity of the fluorescence lifetime of alexandrite decreases with temperature over the region 20–300 °C and its value drops to ~0.3% K^{-1} at 300 °C, compared to ~1.1% K^{-1} at 20 °C. By using a simple two-level kinetic model,[3] the temperature sensitivity can be extrapolated to be ~0.2% K^{-1} and ~0.14% K^{-1} at 400 and 500 °C, respectively, and less than 0.1% K^{-1} at 650 °C. Thus the performance based on the anticipated change of the alexandrite fluorescence lifetime might be expected to be less satisfactory for a thermal sensor operating at higher temperature, e.g., from 500 °C and above due to the poor sensitivity expected from the extrapolation. However, in the recent experimental work of the authors,[8] it has been shown that the temperature sensitivity of the alexandrite fluorescence lifetime starts increasing beyond ~400 °C, i.e., 0.25% K^{-1} at 400 °C to better than 1% K^{-1} over the region from 510 to 700 °C, with ~2% K^{-1} at

 0021-8979/93/073493-06$06.00